A Kinetic Study of Precipitation from Supersaturated Calcium Phosphate Solutions

M. J. J. M. VAN KEMENADE AND P. L. DE BRUYN

Van't Hoff Laboratory, Transitorium 3, Padualaan 8, 3584 CH Utrecht, The Netherlands

Received January 19, 1987; accepted April 13, 1987

The formation of three different crystalline calcium phosphates (DCPD, OCP, HAP) and an amorphous calcium phosphate was studied as a function of pH and supersaturation. Under the experimental conditions the formation of HAP is always found to be preceded by one or more precursors in a sequence that is in agreement with the Ostwald rule of stages. Homogeneous formation of HAP at low concentrations is never observed. A semiquantitative analysis of growth curves and of relaxation times at pH 6.7 and 26°C reveals the growth of OCP to be described best by a mononuclear growth model with fourth-order dependence on the relative supersaturation. The heterogeneous formation of HAP on OCP surfaces is noted to shift to lower α values (reaction extent) with increasing initial supersaturation. It can be described by a polynuclear growth model.

INTRODUCTION

Many investigators have studied the precipitation of calcium phosphates from supersaturated aqueous solutions. Mechanisms of formation of these compounds are of great importance for biological systems like bone and teeth which consist mainly of an apatitic calcium phosphate and for milk in which the main inorganic constituent is calcium phosphate. The major part of the calcium phosphate in milk is linked to the protein casein, thus stabilizing casein micelles in milk. The structure of this micellar calcium phosphate is a subject of great interest and controversy (1–5). Numerous studies have been done on the formation of apatitic phases at physiological pH (7.4). In high or medium supersaturated solutions formation of apatite always seems to be preceded by the precipitation of one or more precursor phases. A list of the different modifications of calcium phosphate which can be formed is given in Table I. Amorphous calcium phosphate, a modification in which no long-range order can be detected by X-ray diffraction studies, has received much attention (6–9). The chemical composition of this glass-like precursor apparently depends on that of the supersaturated solution, although ACP is predominantly formed at higher pH (>7). Studies of Feenstra (10, 11) at pH 7.4 and 8.5 at medium to high supersaturation show that heterogeneous formation of ACP is followed by subsequent nucleation of OCP which serves as a template for HAP formation. At lower pH the formation of HAP is observed to be preceded by OCP or DCPD (13–15). Depending on solution composition and mainly pH both phases can act as a precursor for each other or as a precursor for HAP as pointed out in seeded constant composition experiments performed by Nancollas and co-workers (16, 17). These investigations suggest that by a proper choice of the physical and chemical environment, different modifications (Table I) may be induced to precipitate.

In systems where the different modifications have different solubilities (and therefore different supersaturations), the precipitation order is commonly observed to follow the Ostwald rule of stages (19). This rule predicts that the phase which is thermodynamically least stable will form first. For a complete under-

0021-9797/87 $3.00

TABLE I

Calcium Phosphate Phases

Phase	Composition	Ca/P
Brushite (DCPD)	$CaHPO_4 \cdot 2H_2O$	1.00
Monetite (DCPA)	$CaHPO_4$	1.00
Octacalcium phosphate (OCP)	$Ca_4H(PO_4)_3 \cdot 2.5H_2O$	1.33
Whitlockite/tricalcium phosphate (TCP)	$Ca_3(PO_4)_2$	1.50
Hydroxyapatite (HAP)	$Ca_5(PO_4)_3OH$	1.67
Amorphous calcium phosphate (ACP)	—	—

standing of this rule obviously the kinetic processes must be taken into account.

In Fig. 1 solubility isotherms of HAP, OCP, and DCPD are given at 25 and 37°C as plots of log P_T versus pH where P_T is the total initial phosphate concentration in solution (moles/liter). The chosen ratio (Ca/P) of total calcium to phosphate is 1.16 and the ionic strength is 0.15 *M*. Under these conditions whitlockite and monetite are not found. The solubility products of HAP, OCP, and DCPD and the association constants needed for the calculation of the isotherms are collected in Table AI, Appendix A.

We note that HAP is the thermodynamically most stable phase. At pH 6.7 and a temperature of 26°C the isotherms for OCP and DCPD intersect. Above pH 6.7 DCPD has the higher solubility and is therefore less stable than OCP. At a lower pH the order of increasing stability is OCP < DCPD < HAP. The Ostwald rule would therefore predict a change in the precipitation sequence around pH 6.7 for the composition chosen in constructing Fig. 1. This interesting observation may also be of significance for the micellar calcium phosphate in milk as the pH of milk is about pH 6.7.

The objectives of our study are twofold. First, we wish to study the formation of different calcium phosphates as a function of pH and initial supersaturation to test the validity of the Ostwald rule of stages.

The supersaturation (II) with respect to a given calcium phosphate phase is defined as

$$\text{II} = \frac{\text{ionic activity product (IP) in solution}}{\text{solubility product } (K_{sp})}, \quad [1]$$

where the following IP's are defined,

$$\text{IP}_{HAP} = ([Ca^{2+}]f_2)^5([PO_4^{3-}]f_3)^3 K\omega/[H^+]f_1 \quad [2]$$

$$\text{IP}_{OCP} = ([Ca^{2+}]f_2)^4([PO_4^{3-}]f_3)^3[H^+]f_1 \quad [3]$$

$$\text{IP}_{DCPD} = [Ca^{2+}]f_2[HPO_4^{2-}]f_2. \quad [4]$$

Calculations of solution concentrations were performed by an iterative method described in Appendix A. A second aim of this study is to get information on the kinetics of nucleation and growth of the solid modifications and to compare experimental results with theoretical models.

The experiments were performed at constant pH. This allows one to assume that the

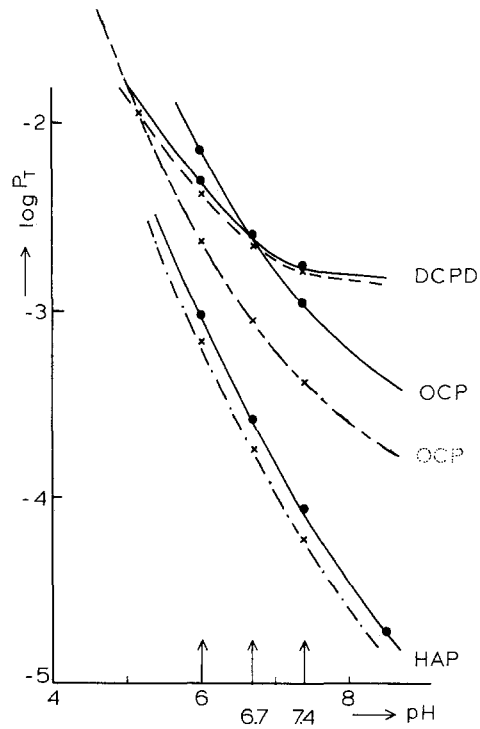

FIG. 1. Solubility isotherms of HAP, OCP, and DCPD at 25°C (solid lines) and 37°C (dotted lines) as log P_T vs pH. P_T is the total phosphate concentration in solution (mole/liter). The chosen Ca/P ratio was 1.16. The ionic strength of the solution I = 0.15 *M*.

interfacial properties remain essentially constant. Precipitation studies were performed at pH 6, 6.7, and 7.4 at a temperature of 26°C. Raising the temperature has the effect of shifting the intersection of the solubility isotherms of OCP and DCPD to a lower pH (Fig. 1). At pH 6.7, 37°C the order of increasing stability is DCPD < OCP < HAP. A series of experiments was therefore also performed at pH 6.7 and $T = 37$°C to study this effect.

EXPERIMENTAL

The relaxation experiments were performed in a thermostated double-walled reaction vessel developed by Vermeulen *et al.* (18). The experiments involve building up a desired supersaturation and then allowing the system to relax at constant pH.

The particular procedure to be followed in building up the supersaturation will be of importance in the relaxation behavior as the formation and growth of nuclei during this stage cannot be ruled out. Two methods are commonly used for mixing the components in order to achieve the desired "initial" supersaturation. A fast injection of a highly concentrated solution of one component into a solution of other components has the advantage of reaching the desired supersaturation very fast. A disadvantage, however, is that small concentrated droplets may exist in the solution for a very short time. At their interface with bulk solution the supersaturation can be so high that a considerable number of nuclei may form. It is possible that the entire nucleation process is restricted to this period. Vigorous stirring is therefore required to reduce the lifetime of the droplets to a minimum. The other method involves a slow addition of a less concentrated solution in order to avoid the high local supersaturations and to accomplish homogeneous nucleation at the intended "initial" pH and supersaturation. The time before achieving the desired supersaturation however can be very long and heterogeneous nucleation cannot be ruled out. This will result in a polydisperse collection of particles whereas by the first method a more monodisperse precipitate will form. In this way the mixing procedure may greatly affect the precipitation process. Different nuclei can be formed under the same "initial" conditions making it possible for different crystal phases to develop by growth. A careful study of mixing procedures is therefore necessary before comparing experimental results from different sources.

In our experiments the supersaturation was always built up by the first method. A solution of KH_2PO_4 (1–15 mM) and $Ca(NO_3)_2$ (1–15 mM) was mixed with a 0.15 M KNO_3 solution. During this mixing the pH is about 4.5 and therefore the solution is still undersaturated with respect to all modifications of calcium phosphate. The desired supersaturation and pH were reached by a fast injection of a 0.5 M carbonate-free KOH solution under nitrogen pressure. The selected pH was always obtained within 1–2 min. The pH was monitored and adjusted with an automatic titrator consisting of an Apple microcomputer, an Ankersmit pH meter, and a Schott automatic buret. During the relaxation the pH was always maintained constant to within 0.003 pH units.

Amagruss type C-1017 combination electrodes were used to measure the pH of the solution. They were calibrated with Electrofact buffer solutions before and after each experiment. Only experiments with an electrode drift in pH less than 0.01 were accepted. Uptake of CO_2 was prevented by bubbling nitrogen gas through the solution. The ionic strength of the solution was kept constant during the precipitation by the presence of 0.15 M KNO_3. The magnitude of the initial calcium-to-phosphate ratio (Ca/P) which is an important parameter in the precipitation of calcium phosphates was chosen between 1.00 and 1.67 but in most experiments was kept at 1.16 ± 0.01. All reagents were of analytical grade and for all solutions twice-distilled, demineralized water was used. Aliquots (100–500 ml) were withdrawn from solution and separated from the solution phase by filtration through 0.65- to 0.10-μm filters. The samples were not washed because of possible preferential dissolution of part of the solid

(7). The precipitates were dried over silica gel using an oil pump and were stored over silica gel. The solid phase was characterized by X-ray diffraction (Guinier–de Wolff camera, Enraf Nonius, employing Cu$K\alpha$ radiation) and the patterns were compared with those tabulated in the JCPDS chart system, by infrared spectroscopy (KBr pellet technique, Perkin–Elmer spectrophotometer), and by scanning electron microscopy techniques (Cambridge stereoscan) for morphology studies. For a semiquantitative analysis of calcium and phosphate content of the samples the microscope was equipped with a Link X-ray microanalysis system.

RESULTS

For each precipitation series performed at a given pH and temperature the effect of initial supersaturation was studied. As precipitation of the solid phase is accompanied by a drop in pH, the extent of the reaction $\alpha(t)$, where $0 \leq \alpha(t) \leq 1$, is measured by the cumulative amount of base added to maintain a constant pH. For a pure phase growing from a stoichiometric solution the extent of reaction is defined by

$$\alpha(t) = \frac{c(0) - c(t)}{c(0) - c(\infty)} \equiv \frac{\mathrm{OH}(t)}{\mathrm{OH}(\infty)}, \qquad [5]$$

where $c(t)$ and $c(\infty)$ are the concentrations of a chosen component in solution at time t and at infinite time (saturation–concentration). $c(0)$ is the initial concentration in solution.

In this complex-precipitating system, however, it is not possible to define a single relationship between the amount of base added and $\alpha(t)$. As the solution and the to be precipitated solid phase have different stoichiometries, $c(\infty)$ will be a function of $c(0)$ and the initial supersaturation. For each experiment with different initial concentrations, $c(\infty)$ or $\mathrm{OH}(\infty)$ must be calculated separately. Another problem arises if different phases with different chemical compositions are growing during one experiment. Depending on the amounts of the different phases forming, the solution composition will alter in a complicated manner. This will affect the saturation concentration $c(\infty)$ of all phases. Furthermore, as the different calcium phosphates have a different alkalinity (DCPD < OCP < HAP), the relationship between the amount of base added and $c(t)$ will be different for each phase. Thus, $\mathrm{OH}(\infty)$ will differ for each phase.

As an operational measure for the progress of the precipitation we shall use the quantity $\mathrm{OH}(t)$ or its normalized equivalent $\mathrm{OH}(t)/\mathrm{P_T}$ where $\mathrm{OH}(t)$ is the cumulative amount of base added (in moles/liter) at time t. Assuming that only one phase is growing we can then calculate the amount of base, $\mathrm{OH}(\infty)$ or $\mathrm{OH}/\mathrm{P_T}$, necessary to reach the saturation limit for that phase for each experiment at a fixed temperature, pH, and initial concentration $c(0)$.

In Fig. 2a a typical example of a relaxation curve for a single growing phase is shown. As a result of an increasing surface area and a decreasing supersaturation during the relaxation a sigmoidal shape of the curve is expected with only one inflection point. At this point, where the growth rate reaches its maximum value the relaxation time t_R, a highly reproducible parameter in precipitation kinetics, is defined. In addition a so-called lagtime t_L is used for analyzing precipitation kinetics. This time parameter is defined as the period before the first base uptake, but is less reproducible and its magnitude will also depend on the experimental detection limit (sensitivity for registering a change in pH). Another relaxation parameter to be used in this study is the total amount of base or $(\mathrm{OH}/\mathrm{P_T})$ added.

For a complex-precipitating system where the precipitation involves growth of more than one phase, the relaxation curve will be more complicated in form and its analysis will not be straightforward. Figures 2b and 2c illustrate such complex, constant pH curves. In Fig. 2b, a two-stage precipitation is shown, where the formation of phase I is followed by the subsequent formation of phase II. This results in two sigmoidal curves where we could define a relaxation time t_R for each precipitating phase. As the formation of the two phases will not be

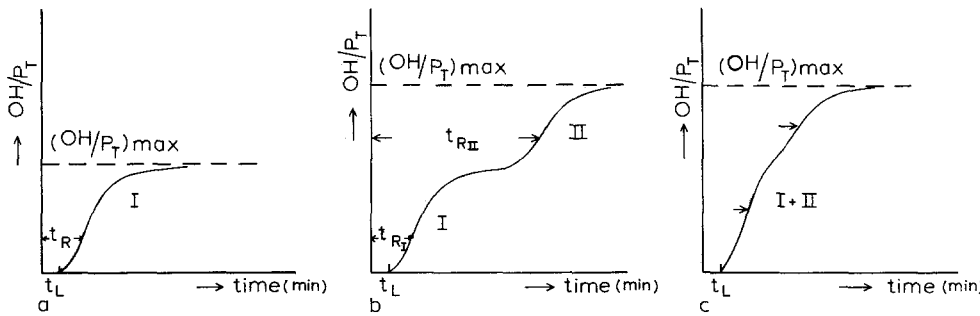

FIG. 2. Typical relaxation curves for precipitation of (a) a pure phase, (b) two phases forming successively, and (c) two phases forming simultaneously over a certain period. Precipitation parameters are the relaxation time (t_R), defined at inflection points of the S-shaped curves, the lagtime (t_L), and the maximum amount of base uptake ($OH(\infty)/P_T$). In curve c arrows point to inflection points which cannot be interpreted as separate relaxation times.

independent, a simple analysis of relaxation time, t_RII, will be difficult. Figure 2c represents a precipitation curve where over a certain period both phases I and II are precipitating simultaneously. This will result in inflection points in the overall growth curve which cannot be interpreted as relaxation times for growth of the phases. The lagtime could also be influenced by the simultaneous growth of two phases in the early stages of the precipitation.

Relaxation Times and Phase Analysis at pH 6.7 and 26°C

Typical examples of relaxation curves are given in Fig. 3. In all cases a measurable lagtime is seen to precede the uptake of base. At high to medium initial supersaturation (curves a–c) a one-stage precipitation takes place where the relaxation time is defined by the inflection point of the curve. The lagtimes and relaxation times are seen to increase with decreasing initial phosphate concentration. Figure 4 illustrates the sharp increase in t_R with initial phosphate concentration. From this plot the kinetic precipitation boundary can be determined. The extrapolated value of 3.9 m*M* for the critical phosphate concentration of this boundary is in agreement with earlier work of Feenstra (10). For all experiments the saturation boundaries with respect to HAP, OCP, and DCPD were calculated assuming the separate formation of each pure phase. At low supersaturations (Fig. 3d) a two-stage precipitation curve of the type presented in Fig. 2c is measured.

Detailed IR and X-ray studies show OCP to be the main precipitating phase at medium supersaturations (curves b and c, Fig. 3). SEM photographs of samples taken in this region show the characteristic globules with the platelike fine structure well known for OCP (Fig. 5c). In experiments at low supersaturation (see Fig. 3, curve d) additional large amounts of brushite are present as large platelets. Figure 5 (electron micrograph a) illustrates the presence of DCPD whereas electron micrograph b shows the presence of OCP globules in the same sample. Both OCP and DCPD are already present before the first inflection point is reached. X-ray microanalysis also indicates that the particles have Ca/P ratios of 1.30 $\pm$ 0.05 and 1.00 $\pm$ 0.05 in agreement with those of the solid phases OCP and DCPD (Table I). At high supersaturations the OCP globules are overgrown with a more alkaline material (Ca/P > 1.5) as is shown in Fig. 5d. At still higher phosphate concentrations HAP could be detected by X-ray diffraction and IR analysis.

Additional information about the nature of the precipitating phases can be obtained from calculated saturation limits, $OH(\infty)/P_T$. Above the saturation limit of a given phase,

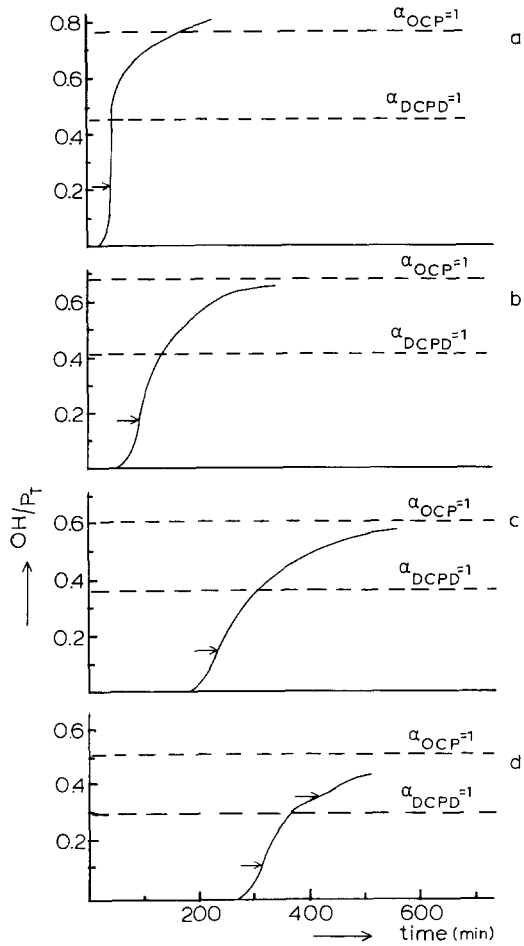

FIG. 3. Relaxation curves, OH/P_T vs time (min), at different initial supersaturations at a constant pH of 6.7, an ionic strength of 0.15 *M*, a Ca/P ratio of 1.16, and a temperature of 26°C. Initial concentrations of phosphate in solution: (a) P_T = 6.29 m*M*, (b) P_T = 5.39 m*M*, (c) P_T = 4.79 m*M*, and (d) P_T = 4.20 m*M*. The dotted lines indicate the saturation boundaries (α = 1) with respect to OCP and DCPD assuming that only the pure modifications are formed. The HAP saturation is reached at a OH/P_T value of 1.40. Arrows point to inflection points in the curves.

uptake of base can be ascribed only to the precipitation of a phase with a lower solubility. At high phosphate concentrations (Fig. 3a) the relaxation curve is seen to rise above the saturation boundary for OCP (α_{OCP} = 1). This observation suggests that, at least in this stage of the reaction, HAP must be forming. At medium concentrations (Figs. 3b and 3c) the relaxation curves rise asymptotically toward the OCP saturation boundary as is to be expected for pure OCP growth. At low supersaturations (curve d) the relaxation tends to approach a lower OH/P_T limit which, however, lies above the DCPD saturation value. It represents a saturation limit for OCP which is lowered because the formation of brushite consumes less base for each phosphate ion removed from solution. The second inflection point occurs slightly above the saturation boundary that was calculated for pure DCPD growth and implies the presence of OCP. This inflection point could be the result of a decreased DCPD growth rate as saturation of DCPD is being approached, while the OCP growth rate still increases.

Relaxation Curves and Phase Analysis at pH 7.4 and 26°C

Two types of relaxation curves (see Fig. 6) can be distinguished at pH 7.4. At high phosphate concentrations (Fig. 6a), a rather smooth

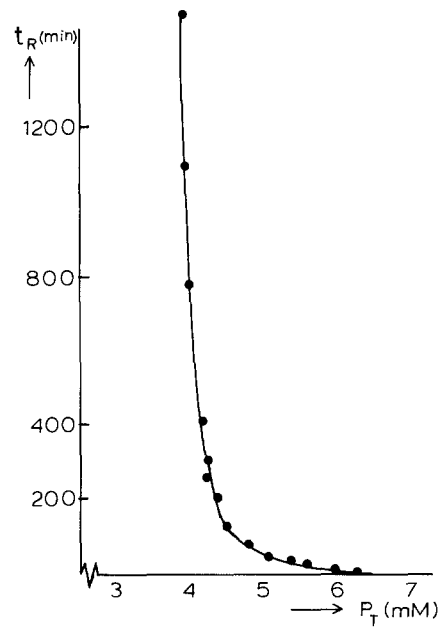

FIG. 4. Relaxation times at pH 6.7, 26°C as a function of total initial phosphate concentration P_T (m*M*), I = 0.15 *M*, Ca/P = 1.16.

S-shaped curve is obtained and in some experiments an extra inflection point is noticeable at a low OH/P_T value. At lower supersaturations (Fig. 6b), a three-stage relaxation behavior is noted. Uptake of base occurs immediately, but then slows down to a near-standstill before slowly rising again and to rise more steeply afterward. The shape of the relaxation curve, characterized by three inflection points, could be accounted for by either the successive or the simultaneous growth of two phases as sketched in Figs. 2b and 2c.

Feenstra (10, 11) also performed relaxation studies at this pH and used the same experimental conditions except for a Ca/P ratio of 1.67. For comparative purposes we performed a few experiments at Ca/P ratios of 1.33 and 1.67. The shape of the relaxation curves at these Ca/P ratios does not deviate markedly from that shown in Fig. 6 except that the near-plateau reached in the first stage at the lower supersaturations (see Fig. 6b) falls at slightly higher levels with increasing Ca/P ratio. This latter observation indicates that a larger amount of the first phase to form is present.

Solid phase analyses show that at high supersaturations OCP was present in the early stages of the reaction. Its presence was mainly detected by X-ray diffraction which showed a double line at 9.37/9.05 Å so characteristic of OCP (100 and 110 planes, respectively). In a later stage only HAP could be detected by X-ray diffraction or electron microscopy. These observations suggest that caution be exercised in using relaxation times as a quantitative measure for the homogeneous growth of HAP. SEM photographs taken in the late stages of precipitation (Fig. 7) show the precipitate to have a spongy texture with a Ca/P ratio between 1.57 and 1.65. Ratios on the order of 1.50–1.65 are often reported for calcium-deficient apatites. Increasing the magnification by a factor 10 showed the same structure without revealing more detail which could possibly indicate a fractal structure. A sufficient resolution to study the morphology of individual crystals could not be obtained. The HAP crystallites (20) are often very small (ranging from 5 to 50 nm). At lower supersaturations (Fig. 6, curve b) X-ray diffraction and IR studies could not detect any crystalline phase during the first stage of the reaction. This suggests that the growth of ACP be responsible for the uptake of base. In the second stage, the region between the first two inflection points in Fig. 6b, OCP could be detected by X-ray diffraction while in the late stage only HAP was noted. Beyond the last inflection point only HAP growth ocurs. Similar results were obtained by Feenstra (10).

From Fig. 6 we note that the precipitation of HAP is apparently terminated long before the calculated saturation boundary for HAP is reached and even before the saturation limit for OCP. This behavior cannot be explained by the earlier precipitation of some OCP. A possible explanation for this behavior must be found in the existence of a kinetic boundary for growth or to a very slow growth of HAP in this range of supersaturation. DCPD was never detected over the whole supersaturation range at pH 7.4.

Relaxation at pH 6.0 and 26°C

The precipitations can all be characterized by a single-stage S-shaped relaxation curve. However, at high supersaturations ($P_T \geqslant 15$ mM) the relaxation curves rise above the DCPD saturation boundary. Although the only detectable phase at the end of the precipitation was DCPD, an amount of OCP could

FIG. 5. Scanning electron microscopic (SEM) photographs at pH 6.7 and 26°C. (a) Large DCPD platelets with OCP at low supersaturation. (b) More representative picture of characteristic OCP globules with fine platelet structure at low supersaturation. (a and b taken from the same sample in the early stages of the reaction.) (c) OCP at medium supersaturation. (d) OCP crystals overgrown with apatitic material (Ca/P > 1.50) at high supersaturation in the late stage of the reaction.

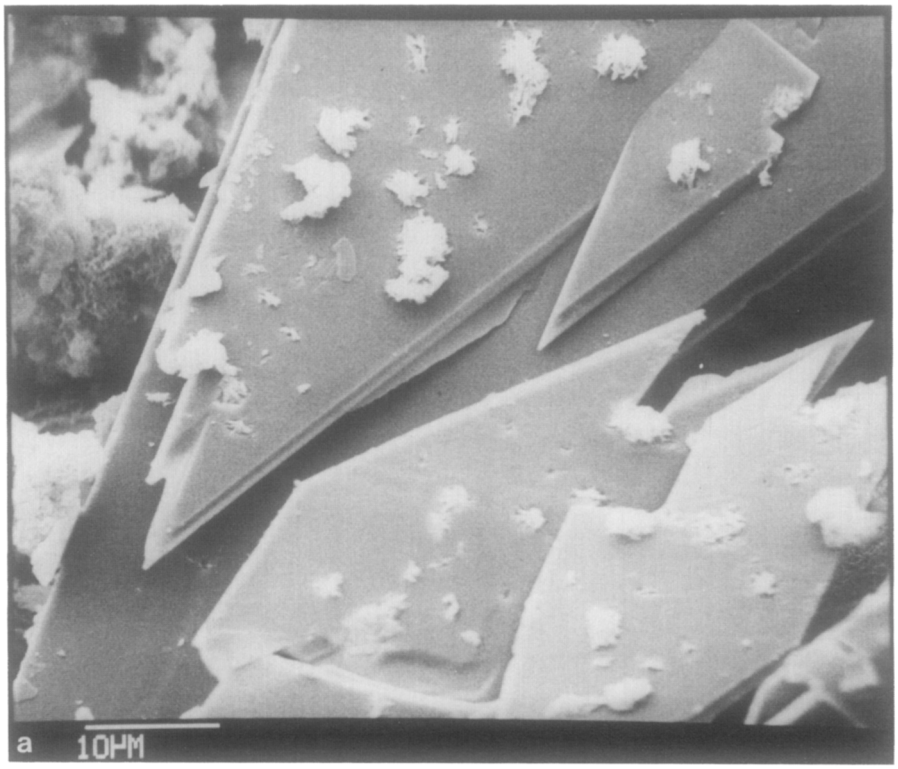
a
10μM

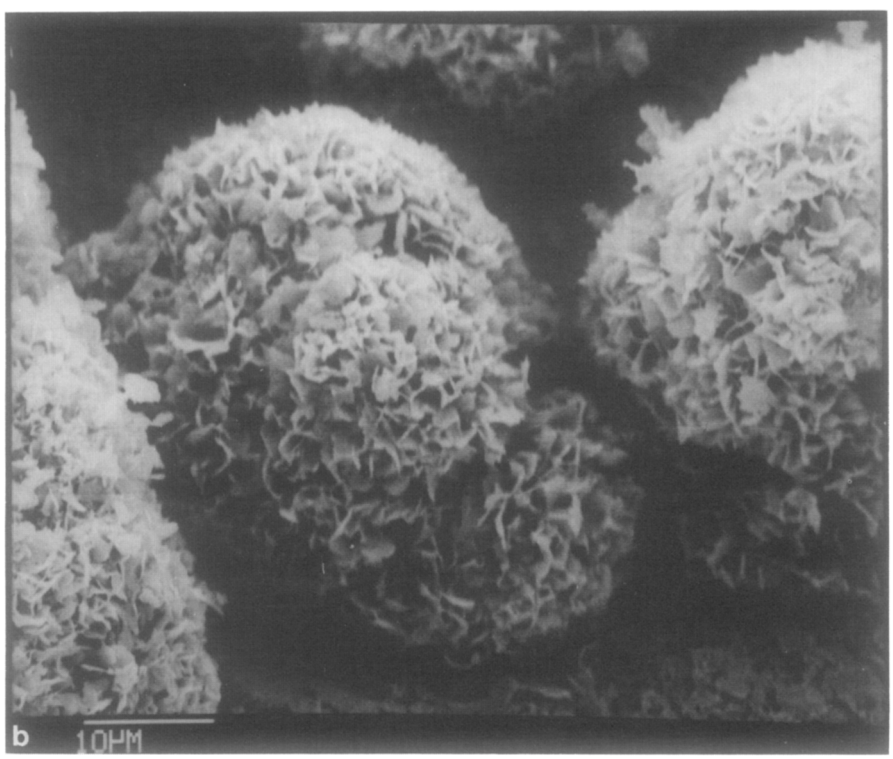
b
10μM

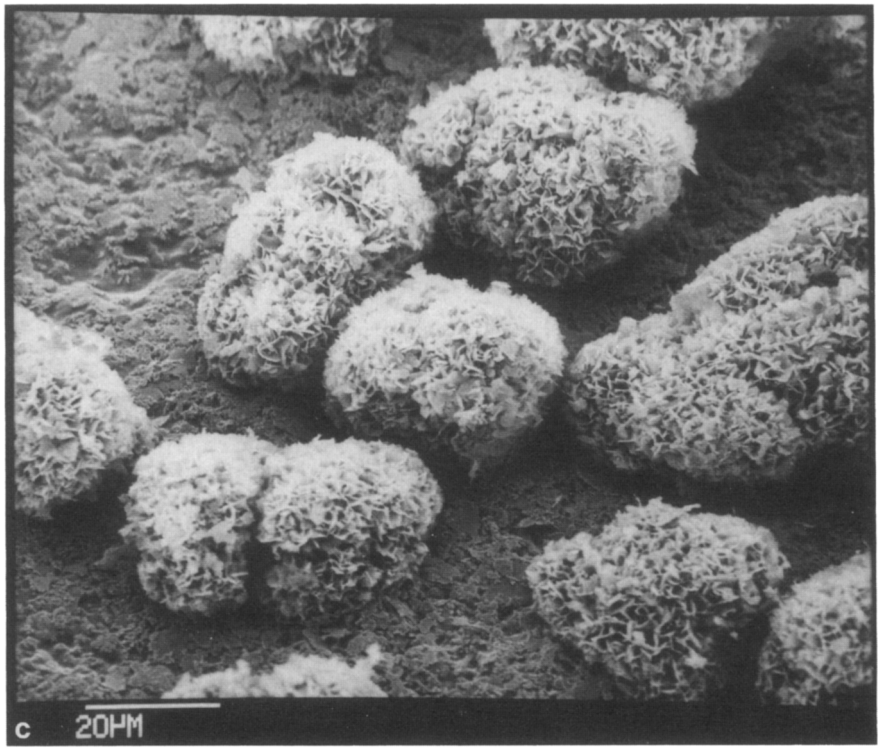

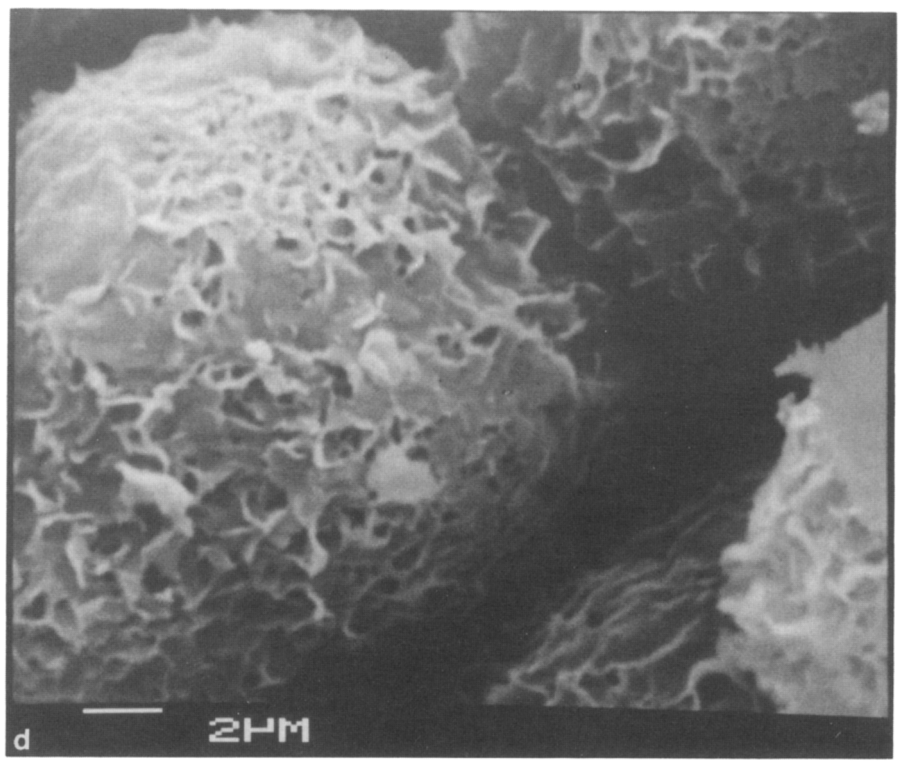

FIG. 5—*Continued.*

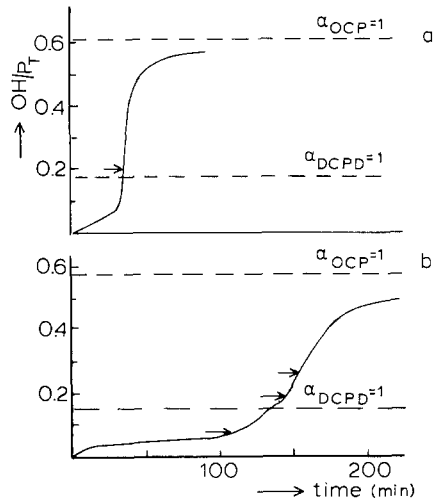

FIG. 6. Typical relaxation curves (OH/P_T vs time (min)) as a function of initial supersaturation at a constant pH of 7.4. $I = 0.15$ M, $T = 26°C$, and the Ca/P ratio = 1.16. Initial phosphate concentrations: (a) $P_T = 3.28$ mM, (b) $P_T = 2.84$ mM. Arrows point to inflection points in the relaxation curves. The saturation limit of HAP is reached at a OH/P_T value of 1.15.

be observed in the early stages of the precipitation. The precipitation order at these conditions is thus OCP → DCPD. DCPD takes over growth without detectable changes in rate of base uptake. At low supersaturations ($P_T \leq 12.5$ mM) only DCPD could be detected. The curves rise toward the saturation boundary for pure DCPD growth.

Relaxation at pH 6.7 and 37°C

Relaxation curves at pH 6.7 and a temperature of 37°C are presented in Fig. 8. The curves show the same general features as noted at pH 6.7 and 26°C (Fig. 3). At the higher supersaturations (Figs. 8a and 8b) the curves again are S-shaped with only one inflection point. The main difference is seen at low supersaturations (curve c). Again a two-stage precipitation is indicated, but the stages appear to be better separated. This observation suggests that two phases form and grow separately

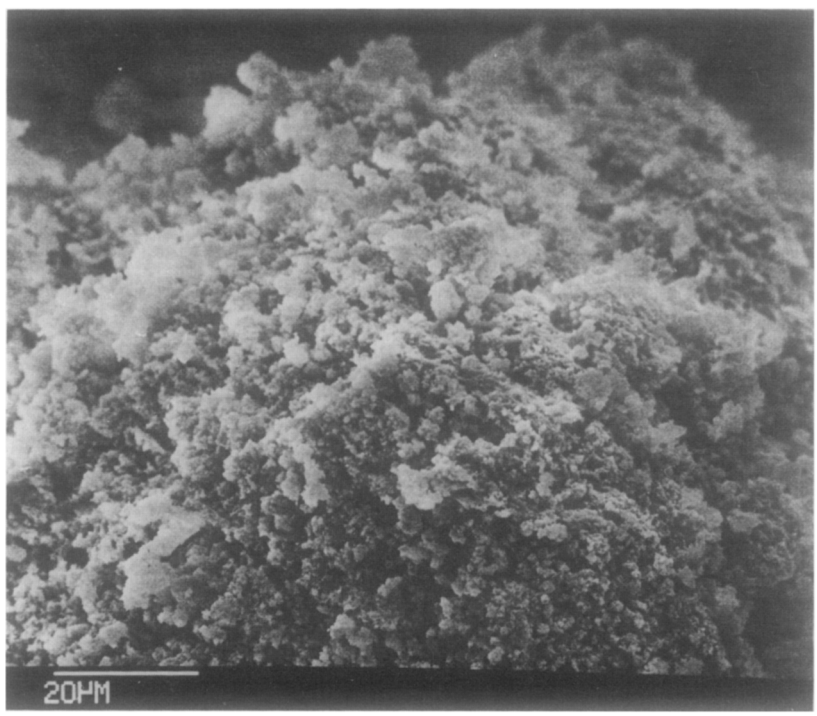

FIG. 7. SEM photograph of an apatitic phase developed at pH 7.4 and high supersaturation (see Fig. 6, curve a). The measured Ca/P ratio (X-ray microanalysis, Link system) of the solid varies from 1.57 to 1.65.

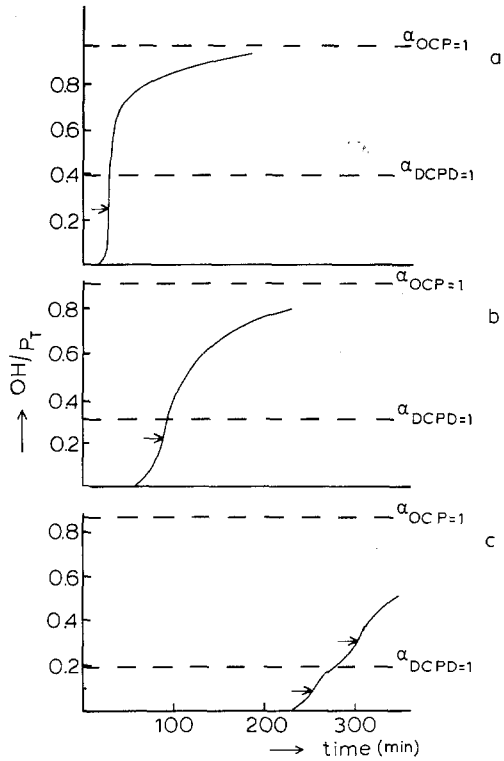

FIG. 8. Typical relaxation curves at pH 6.7 and 37°C as a function of supersaturation. $I = 0.15$ M, Ca/P = 1.16. Initial phosphate concentrations: (a) $P_T = 4.5$ mM, (b) $P_T = 3.9$ mM, and (c) $P_T = 3.0$ mM. Arrows point to inflection points in the relaxation curves. The saturation limit of HAP is reached at a OH/P_T value of 1.31.

and in succession (compare with Fig. 2b). The first stage just reaches the DCPD saturation boundary and we may conclude tentatively that only DCPD grows during this stage. This conclusion is in agreement with SEM photographs taken in the early stages of the precipitation, where only DCPD crystals could be detected (Fig. 9a) in contrast to the observations at 26°C (Figs. 5a and 5b). Electron micrographs taken during the second stage of precipitation show both OCP and DCPD to be present (Fig. 9b). The OCP crystals appear to form only on the surface of DCPD crystals. At intermediate supersaturation (Fig. 8, curve b) only OCP could be detected whereas at high supersaturations (curve a) HAP is the dominating phase.

DISCUSSION

Precipitating Sequence

The precipitating sequences observed under the different experimental conditions are summarized in Table II.

A comparison of the information in Table II with the solubility isotherms in Fig. 1 shows, without exception, that the order within which the solid phases precipitate is also that of increasing phase stability under the specified experimental conditions. The reversal in the precipitation of the first phase at pH 6 and 26°C compared to that at pH 6.7 and 37°C, especially, provides a striking confirmation of this general observation. At pH 7.4 where one would expect DCPD to be the first precipitating phase, the much less stable ACP takes over as precursor. The Ostwald rule of stages (19) is thus well obeyed by precipitation from supersaturated calcium phosphate solutions. A satisfactory explanation of this rule, which clearly must be based on kinetic arguments, is less readily available, when one considers that the thermodynamically most stable phase will have the highest degree of supersaturation in a solution supersaturated with respect to all possible solid modifications.

Stranski and Totomanov (21), Gutzow and Toschev (22), Feenstra (11), and Van Straten (12) provided kinetic arguments largely based on classical nucleation theory (23, 24) and induction times derived from an analysis of nonsteady-state nucleation to explain observed precipitation sequences. Clearly growth rates (24–26) should also be taken into account, especially when at relatively high supersaturations the decision as to which phase would eventually develop cannot be taken in the nucleation stage.

As already mentioned it is very likely that nucleation occurs during the mixing stage. Experimental indications for this assumption were obtained from relaxation time studies which showed a dependence of t_R on mixing speed and concentration of titrant. If nucleation is indeed restricted to the mixing period, a flash-like formation of very small critical

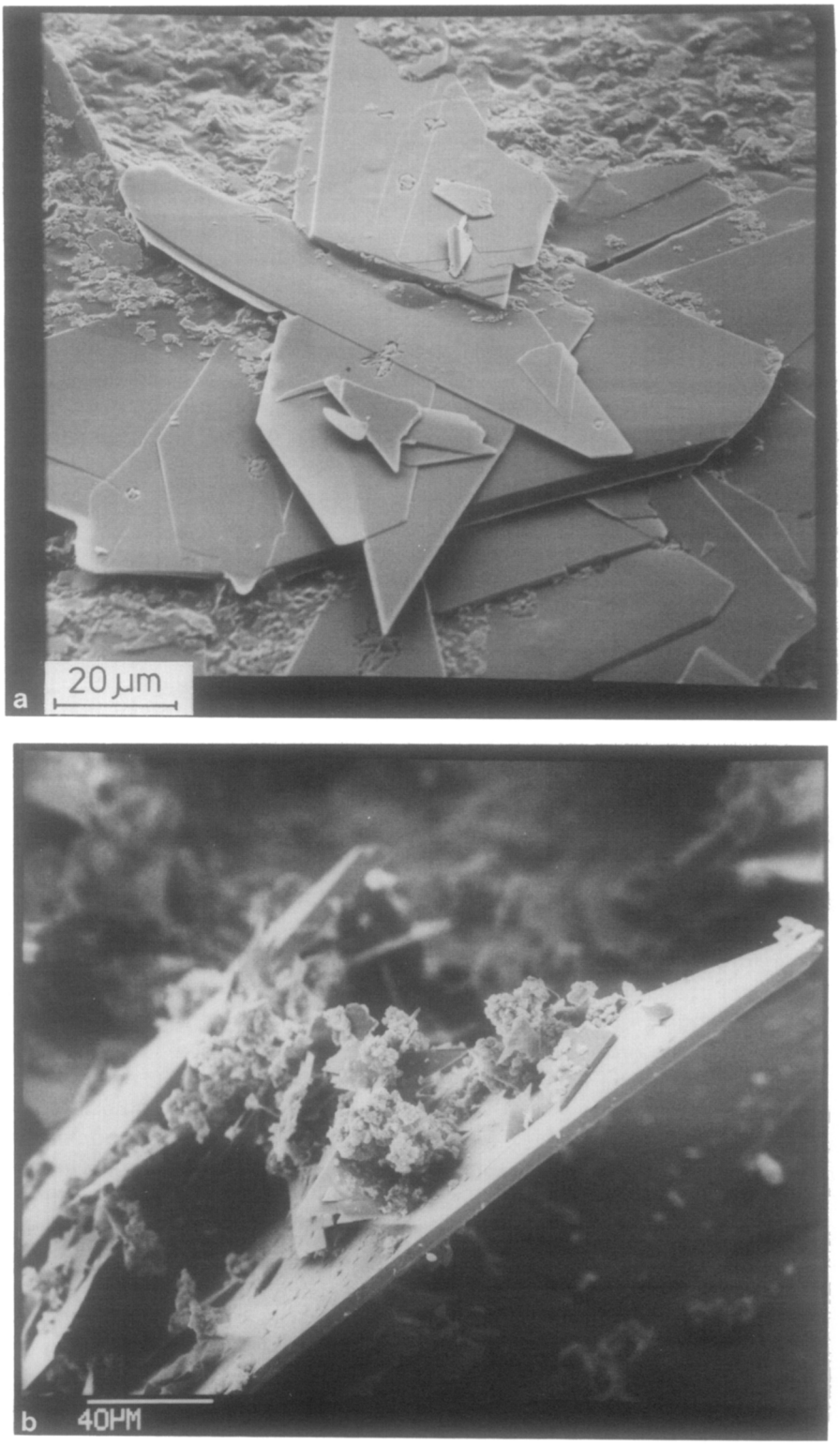

FIG. 9. SEM photographs taken at pH 6.7, 37°C at low supersaturation (P_T = 3.0 mM). (a) Early stages of precipitation where only DCPD crystals are detected. (b) Late stages where both DCPD and OCP are present. The OCP crystals seem to have developed only on DCPD surfaces.

TABLE II

Precipitating Sequences

pH	T(°C)	Precipitating sequence
6.7	26	DCPD = OCP → HAP
7.4	26	ACP → OCP → HAP
6	26	OCP → DCPD (→) HAP
6.7	37	DCPD → OCP → HAP

nuclei would occur at very high local supersaturation when phase distinguishability is unlikely.

At medium supersaturations the surfaces of the growing crystalline particles will be relatively smooth and growth will proceed by a layer mechanism that requires the formation of a surface nucleus. The flux of surface nuclei (23, 24) is given by

$$J_{2D} = A \exp\left(-\frac{B\sigma^2}{\ln \Pi}\right) \qquad [6]$$

with Π the supersaturation, σ the interfacial tension, and B a factor dependent on temperature, molecular volume, and particle shape. The argument of the exponential term is the free energy, ΔG_{2D}, of formation of a surface nucleus and A is a kinetic factor describing the mechanism for the incorporation of monomers into the growing crystal. This preexponential factor is of crucial importance in explaining the precipitation sequence as the supersaturation in the exponential term will always favor the formation of the thermodynamically most stable phase.

The kinetic factor A will always be larger for an amorphous phase than for a crystalline phase. The surface of the former phase will be rough because of the more disordered structure. Growth will proceed continuously because surface nucleation is not essential and the rate will be limited largely by diffusion of growth units to the surface. The observation that ACP starts to grow immediately after the initial supersaturation has been established at pH 7.4 supports this kinetic argument.

An explanation for the preferred prior precipitation of one crystalline phase to another crystalline phase is less obvious. According to Nielsen and Söhnel (27, 28) a lower interfacial tension or edge-free energy is to be expected for a more soluble phase. This could result in a lower ΔG_{2D} in spite of the lower supersaturation II. A more important factor will probably be the surface roughness that will increase with decreasing interfacial tension resulting in a higher incorporation rate of monomers. The importance of surface roughness for crystal growth rates is confirmed by computer simulations of the growth process by Gilmer and Bennema (29). The kinetic factor A will thus favor the phase with the higher solubility. The precipitating sequence will be determined by the relative magnitudes of the parameters A, σ, and II. Why this apparently always results in sequences following the Ostwald rule is not clear.

At low supersaturations homogeneous formation of the most stable phase (HAP) is to be expected as the solution would be saturated or even undersaturated with respect to the other phases. Direct precipitation of HAP was described by Boskey and Posner (30). In our experiments HAP was never observed to form homogeneously. HAP growth was always preceded by formation and growth of precursors. The precursor phase will influence the kinetics of the precipitation of subsequent phases by serving as template material for heterogeneous nucleation of these phases and their further growth. On the other hand, the solution composition and therefore the supersaturation with respect to other solid modifications will also be modified by the precipitation of a precursor phase. In this respect, a change in the Ca/P ratio (31) during precipitation will be of great importance in the calcium phosphate system where the different crystalline modifications all have different calcium and phosphate contents (see Table I). By varying the Ca/P ratio the supersaturations of the different phases can be decreased or increased. If in the late stage of precipitation, a phase with a Ca/P ratio different from that of the solution forms, one of the lattice ions will become exhausted in solution. This will result in a strong retardation

of the growth of this phase and in changes in the supersaturation with respect to other phases. Clearly a different saturation boundary will also be reached depending on the prevailing Ca/P ratio. A nonstoichiometric Ca/P ratio in solution could also lead to excess adsorption of the more abundant lattice ion at the surface of the growing crystal, thereby lowering the surface energy.

In our experiments an initial Ca/P ratio of 1.16 was usually elected. At pH 6.7 and 37°C, DCPD was the first phase to form (see Table II). The Ca/P ratio in the solution therefore increased with the result that the supersaturation with respect to OCP and HAP decreased less rapidly than that of DCPD during the latter's growth period. The formation of OCP and HAP (probably by heterogeneous nucleation) was therefore favored by growth of DCPD. If OCP were to form first, as in the experiments of pH 6, the opposite will happen. The Ca/P ratio will drop and the supersaturation of DCPD relative to that of OCP will rise. The formation of this more acidic phase will be favored. By choosing a value for Ca/P between 1.0 and 1.33 (for example, Ca/P = 1.16) one would, in general, expect both OCP and DCPD to form, as was indeed observed. A variation of the initial Ca/P ratio at pH 7.4 from 1.16 to 1.67 showed a larger amount of ACP to form with increasing Ca/P ratio. Although the composition of ACP is known to be dependent on solution composition, this could point to a possible preferential formation of this amorphous solid at higher Ca/P ratios.

Analysis of Growth Curves

Direct information on the nucleation step during precipitation is well-nigh impossible. Nucleation consumes only small amounts of the precipitating species that cannot be detected by the measuring technique (change in pH). The measured uptake of base during the constant pH relaxation is thus almost entirely the result of growth processes. For a set of monodisperse, isotropic particles growing according to a diffusion-controlled, mononuclear or polynuclear mechanism the relation between the extent of the reaction (α) and the time (t) can be described (see Appendix B) by the general semiempirical growth equation

$$\dot{\alpha} = K\alpha^n(1-\alpha)^m, \qquad [7]$$

where K is a rate constant which has a different value for each growth mechanism, and n and m are constants the values of which also depend on the particular growth model as shown in Table III.

The term α^n in Eq. [7] describes the dependence of the growth rate on the available surface area or the size of the monodisperse particles and is very sensitive to the magnitude of n at low α values, $0 \leqslant \alpha \leqslant 0.2$. The value of the exponent n is of particular interest in discriminating among the different growth models. The term $(1-\alpha)^m$ gives the dependence of the growth rate on the decreasing supersaturation during relaxation. It becomes the controlling factor at relatively high α values ($\alpha \geqslant 0.5$) when the α^n term approaches a near-constant value regardless of the value of n. We also note that for the two surface nucleation-controlled models, m can vary in magnitude. Its value increases with decreasing supersaturation.

A plot of α versus t according to Eq. [7] yields an S-shaped curve characteristic of many experimental relaxation curves. Another characteristic feature is the inflection point which locates the relaxation time t_R (see Fig. 2a). The value of α at the inflection point can be obtained by applying the condition $d\dot{\alpha}/dt = 0$ and is seen to have the following dependence on the exponents n and m:

TABLE III

Values of n and m according to Eq. [7] for Different Growth Models

Growth model	n	m
Diffusion-controlled	$\frac{1}{3}$	1
Polynuclear	$\frac{2}{3}$	Variable
Mononuclear	$\frac{4}{3}$	Variable

$$\alpha(t_R) = \frac{n}{n+m}. \qquad [8]$$

In Table IV we illustrate that $\alpha(t_R)$ has a single characteristic value for a diffusion-controlled growth mechanism but, as expected, will have different values depending on the magnitude of m for the other growth mechanisms.

In order to identify the growth mechanism(s) responsible for the observed relaxation behavior we use Eq. [7] to fit the relaxation curves to straight lines. This may be done by plotting $\log(\alpha^{-n} \cdot \dot{\alpha})$ versus $\log(1-\alpha)$ for $n = \frac{1}{3}$, $\frac{2}{3}$, and $\frac{4}{3}$ and assuming m to be constant. The latter assumption is justified in the case of the layer growth mechanisms (mono- and polynuclear) if the concentration of the precipitating species does not change by more than one decade in the relaxation experiment. In our experiments the concentration varied by less than a decade, mostly by a factor of 3 to 4.

A typical example of such plots for experiments at pH 6.7 and 26°C is shown in Fig. 10. At this pH and medium initial supersaturations (Figs. 3b and 3c) mainly one phase (OCP) has been identified which justifies the proposed growth analysis. The extent of the reaction, $\alpha = \mathrm{OH}(t)/\mathrm{OH}(\infty)$, was therefore calculated with respect to OCP with $\alpha = 1$ at OCP saturation.

TABLE IV

Points of Inflection according to Eq. [8] for Different Growth Models and Values of m

Growth model	n	m	α
Diffusion	$\frac{1}{3}$	1	0.25
Polynuclear	$\frac{2}{3}$	1	0.40
		2	0.25
		3	0.18
		4	0.14
		5	0.12
Mononuclear	$\frac{4}{3}$	1	0.57
		2	0.40
		3	0.31
		4	0.25
		5	0.21

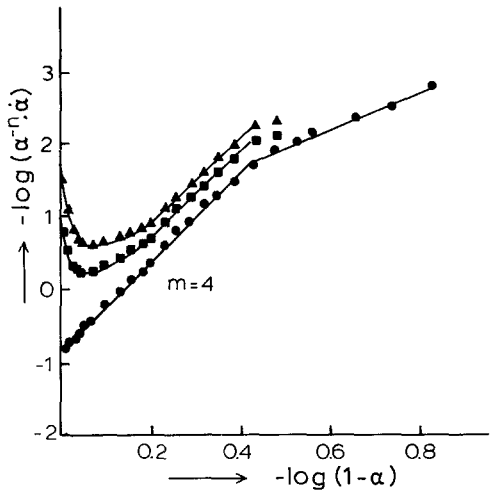

FIG. 10. A typical plot of $-\log(\alpha^{-n} \cdot \dot{\alpha})$ vs $-\log(1-\alpha)$ for a relaxation curve at pH 6.7, $P_T = 5.39$ mM, and a temperature of 26°C for different values of n: (▲) $n = \frac{1}{3}$, (■) $n = \frac{2}{3}$, (●) $n = \frac{4}{3}$.

A straightline is obtained for $n = \frac{4}{3}$. Marked deviations from a straightline can be seen for $n = \frac{1}{3}$ and $n = \frac{2}{3}$ at low α. This suggests that the growth rate is controlled by surface nucleation based on the mononuclear growth model. All three plots yield straight lines with slope $m = 4$ at higher α values when the term $(1-\alpha)^m$ in Eq. [7] dominates. The value $m = 4$ agrees with that earlier observed by Heughebaert and Nancollas (32) for seeded OCP growth at pH 6.0. The growth rate of OCP under these experimental conditions is thus best described by the relation

$$\dot{\alpha} = K\alpha^{4/3}(1-\alpha)^4. \qquad [9]$$

A check on the validity of Eq. [9] is obtained when we note that the experimental relaxation curve has its inflection point at $\alpha(t_R) = 0.25$. This value is consistent with that predicted by Eq. [8] given the values for n and m. It should be noted with reference to Table IV that other combinations of n and m will also yield $\alpha(t_R) = 0.25$.

This analysis is based on the assumption that the growing particles are reasonably monodisperse. If the particles were initially polydisperse the polydispersity should increase

in time when growth proceeds by a mononuclear mechanism (see Appendix B) and the validity of the proposed analysis may be questioned. From Fig. 5 we note that samples taken in the later stages of relaxation are reasonably monodisperse. On assuming, as indicated by the analysis, that the growth is proceeded by a mononuclear mechanism, we conclude therefore that the initial particle size distribution was very narrow. This suggests that a sudden burst of nucleation is responsible for the creation of the growing particles and in turn supports our contention that nucleation occurred in a flash-like manner during the experimental mixing step for building up the supersaturation.

In Fig. 10 we note a sharp break in the straight line plot at high α ($\alpha \approx 0.75$) to yield another straight line with a lower slope.

This break is seen to move progressively to lower α values (higher supersaturation) with increasing initial supersaturation. Three different explanations may be offered for the observed break in the plots: (a) a change in OCP growth mechanism; (b) a change in m, not in growth mechanism; and (c) the occurrence and growth of a new phase. At low supersaturations growth of a solid phase can be accounted for by the presence of screw dislocations; however, the observation that with increasing $\Pi_{initial}$ the break shifts toward higher supersaturation eliminates this possibility (explanation (a)). The observation that m is lower after the break, which is not to be expected when the supersaturation is decreasing, argues against explanation (b) and we are left with possibility (c).

Our experimental observations suggest that growth of HAP in the late stages of the precipitation reaction may be responsible for this break. When HAP starts to grow, a discontinuity in the plots of Fig. 10 is likely because a different growth rate dependence on supersaturation is expected. This prediction is supported by experiments at higher initial supersaturations where increasing amounts of HAP in the later relaxation stage have been detected. Increasing the initial supersaturation leads to the formation of more and smaller particles (the critical nucleus size decreases) with a larger total surface area at a given α. As HAP forms heterogeneously on the OCP surface, this will encourage HAP growth and we can expect HAP to grow at a lower α value. The break in the plots therefore shifts to lower α values as is indeed noted in Fig. 11. We also note that an initial slope of $m = 4$ is observed over the whole supersaturation range. No significance should be attached to the value of the slopes of the straight lines beyond the break as the plotted α has been calculated on the assumption that OCP and not HAP is the growing solid phase.

In Table V the dependence of the position of the break in the straightlines (α_{break}) on supersaturation is listed. We note that at the highest supersaturation values (experiments d and e), $\alpha_{break} < \alpha(t_R) = 0.25$. One would therefore expect that when HAP already starts to grow in the early stages of the relaxation process, this should be reflected in an analysis of the relaxation time t_R.

In the mononuclear growth model the growth rate is largely determined by the frequency with which a surface nucleus forms on a surface of known area. The linear growth rate (dr/dt) (24, 26), assuming the particles to

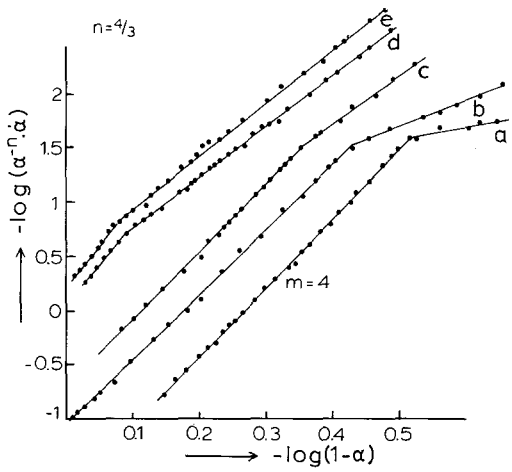

FIG. 11. Plots of $-\log(\alpha^{-n} \cdot \dot{\alpha})$ as a function of increasing supersaturation for $n = \frac{4}{3}$. (a) $P_T = 4.8$ mM, (b) $P_T = 5.4$ mM, (c) $P_T = 5.6$ mM, (d) $P_T = 5.9$ mM, and (e) $P_T = 6.3$ mM.

TABLE V

α_{break} as a Function of Initial Phosphate Concentration and OCP Supersaturation

Exp.	P_T (mM)	$\Pi_{OCP,\,initial}$	$\alpha_{break,\,OCP}$
a	4.8	71	0.75
b	5.4	148	0.65
c	5.6	185	0.56
d	5.9	260	0.20
e	6.3	397	0.13

be monodisperse (due to creation by a flash nucleation), is then given by the relation (see Appendix B)

$$\dot{r} = \beta r^2 d J_{2D}, \qquad [10]$$

where βr^2 represents the surface area of each layer of thickness d, J_{2D} is the flux of surface nuclei, and β is a shape factor. This expression may be integrated to yield

$$\left(\frac{1}{r(0)} - \frac{1}{r(t)}\right) = \beta d J_{2D} t. \qquad [11]$$

If we define somewhat arbitrarily a relaxation time at a certain size $r(t) \gg r(0)$ then, on combining Eqs. [11] and [6] we derive (24)

$$t_R \propto [J_{2D} \cdot r(0)]^{-1}$$
$$\propto r(0)^{-1} \cdot A^{-1} \exp(\Delta G_{2D}/kT). \qquad [12]$$

We may take $r(0)$ (the initial size of the particle when the mononuclear growth model becomes applicable) approximately equal to the critical 3D nucleus radius at the initial supersaturation. The dependence of $r(0)$ on the supersaturation is then given by the Kelvin equation, $r(0) \propto \sigma/\ln \Pi$, a rather weak function of Π compared to the argument of the exponential term in Eq. [12]. Over a limited supersaturation range we may then write Eq. [12] in the form

$$t_R = C \exp\left(\frac{B\sigma^2}{\ln \Pi}\right), \qquad [13]$$

where C and B are constants at a given temperature.

The validity of Eq. [13] for relaxation experiments at pH 6.7 and 26°C where OCP has been shown to be the only growing phase is tested in Fig. 12. A plot of $\ln t_R$ versus $(\ln \Pi_{initial})^{-1}$ (OCP) yields a straight line over a wide range of supersaturation as predicted by Eq. [13] and supports the proposed mononuclear growth mechanism.

We also note a discontinuity in the plot in the neighborhood of $(\ln \Pi_{OCP})^{-1} \approx 0.183$ or $\Pi_{OCP} \approx 240$. This discontinuity coincides with the supersaturation at which the earlier discussed α_{break} drops below $\alpha(t_R)$ (see Table V). The observation of this discontinuity and its location in the plot of Fig. 12 confirm our conclusion that at a certain supersaturation HAP growth occurs even before the relaxation time, defined at the inflection point ($\alpha(t_R) = 0.25$), is reached. A different dependence of t_R on Π is then logical. At high Π (>240) the inflection points cannot be interpreted as OCP relaxation times because two phases already are present in the early stages of precipitation. It should be noted that even at the highest initial supersaturation ($\Pi_{OCP} \approx 400$), when t_L

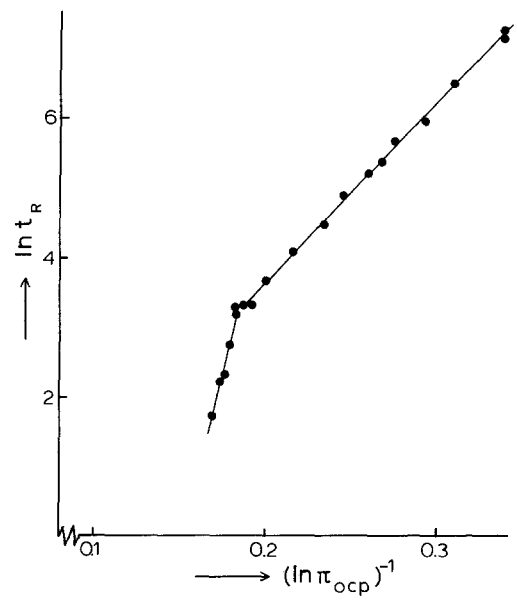

FIG. 12. Relaxation times as a function of initial OCP supersaturation ($\ln t_R$ vs $(\ln \Pi_{OCP})^{-1}$) for experiments at pH 6.7, 26°C. Initial phosphate concentrations vary from $P_T = 3.9$ mM to $P_T = 6.3$ mM. A discontinuity in the plot is noted at $(\ln \Pi_{OCP})^{-1} = 0.183$, $\Pi_{OCP} \approx 240$.

= 0, the initial phase to grow is OCP as is shown by the observed $\alpha_{break} = 0.13$ (see Table V). The growth of HAP apparently requires at all times the presence of a precursor. Similar results were obtained by Termine *et al.* (33) who studied the lifetime of an ACP precursor as a function of supersaturation. They found both the lagtime and lifetime of ACP to decrease at higher supersaturations. The decrease in lifetime was the result of an earlier onset of HAP growth.

Heterogeneous Growth of HAP

Heterogeneous formation of HAP largely determines the relaxation behavior at high supersaturations. In attempting to analyze the relaxation curves under these conditions the correct definition of α_{HAP} must be given. As a result of OCP growth the solution concentrations have decreased and because the Ca/P ratio of the solution is not equal to the stoichiometry of HAP, the saturation concentration $c'(\infty)$ of apatite will depend on the amount of OCP already formed. Assuming that up to a value of α equal to α_{break} (see Fig. 11 and Table V) only OCP grows and thereafter pure HAP growth follows, then both $c'(0)$ (or the concentration of calcium and phosphate) at α_{break} and $c'(\infty)$ can be evaluated. The extent of the reaction can then be defined as

$$\alpha_{HAP} = \frac{c'(0) - c'(t)}{c'(0) - c'(\infty)}, \qquad [14]$$

where α_{HAP} varies between 0 and 1 during the heterogeneous growth. However, because HAP grows heterogeneously on the OCP surface, this surface must also be taken into account. The surface dependence is not described properly by the term α_{HAP} which equals zero at the onset of HAP growth, but must contain an extra contribution of the OCP surface already present. The kinetic growth expression therefore reads

$$\dot{\alpha}_{HAP} = k(\alpha'_{HAP})^n(1 - \alpha_{HAP})^m; \quad 0 \leq \alpha_{HAP} \leq 1, \qquad [15]$$

where

$$\alpha'_{HAP}(t) = \alpha_{HAP}(t) + \alpha_0. \qquad [16]$$

In Eq. [16], α_0 is the surface area of the solid phase at the onset of HAP growth normalized with respect to the total surface area due to HAP growth. The amount of HAP formed may be calculated from the difference $c'(0) - c'(\infty)$ and the amount of OCP from the difference $(c(0) - c_{break})$. The surface areas are then determined by using values of 8 and 36 m^2/g for the specific surface of OCP and HAP, respectively, as obtained from BET gas adsorption measurements. We note that in the evaluation of α'_{HAP} lattice misfit between OCP and HAP is not considered.

In Fig. 13 we give plots similar to those in Figs. 11 and 12 but based on the heterogeneous growth expression, Eq. [15]. At low supersaturations (Fig. 13a) straight lines are obtained for both $n = \frac{4}{3}$ and $n = \frac{2}{3}$ but not for $n = \frac{1}{3}$. At high supersaturations (Fig. 13b) where HAP already starts to grow at low α values the experimental data best fit a polynuclear growth model with a constant value of $m = 10.0 \pm 0.5$. No quantitative significance should be attached to the absolute value for m (considering the assumptions made in the formulation of Eq. [15]) although it is interesting to note that a value of 10 was also reported for apatite growth at pH 6.7 by Feenstra (10).

CONCLUSIONS

The observed precipitation sequence is dictated by the relative solubility of the different solid phases at a fixed pH and temperature and is in accord with the Ostwald rule of stages. This rule is obeyed regardless of the solution conditions under which the relaxation was conducted. A reasonable explanation of the observed precipitation behavior must consider the kinetics of the process and more specifically the rate of growth of phases in the early stages of relaxation.

Homogeneous formation of HAP at low supersaturations is never seen. The development of this phase is always preceded by the

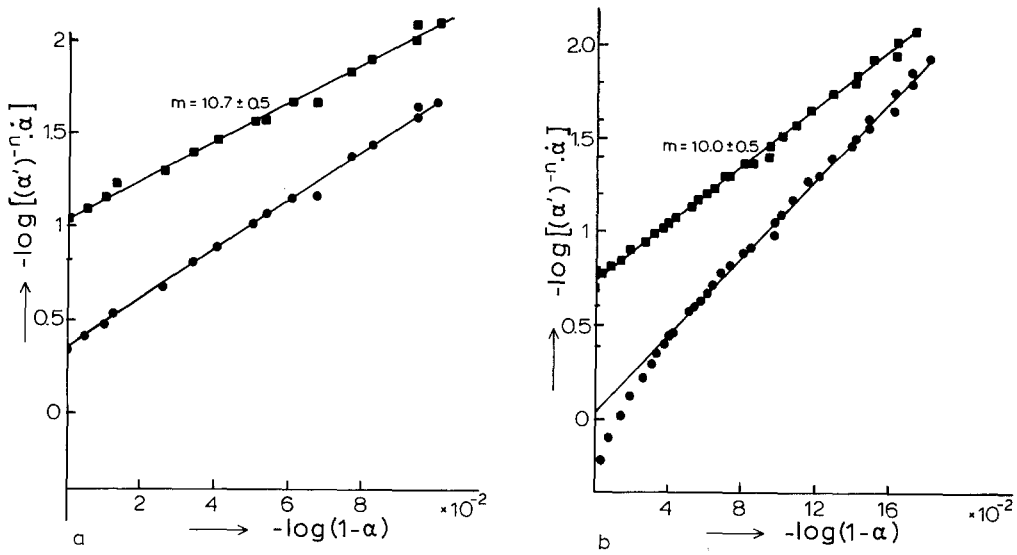

FIG. 13. Plots of $-\log[(\alpha')^{-n} \cdot \dot{\alpha}]$ vs $-\log(1 - \alpha)$ according to Eq. [15] for the heterogeneous growth of HAP at two initial concentrations: (a) $P_T = 5.4$ mM, (b) $P_T = 6.3$ mM (curves b and e, Fig. 11, respectively). (■) $n = \frac{2}{3}$, (●) $n = \frac{4}{3}$.

formation and growth of one or more precursor phases.

At pH 6.7 and 26°C OCP was observed to form at medium supersaturation largely to the exclusion of other phases. The growth curves (α vs t) and relaxation times (t_R) obtained under these conditions were analyzed semiquantitatively by application of classical nucleation and growth theories. The analysis reveals that the kinetics of formation of OCP is best described by a flash-like nucleation step in combination with surface nucleation-controlled growth based on the mononuclear growth model.

In the later stages of the constant pH relaxation HAP forms heterogeneously on the OCP surface. With increasing initial supersaturation the onset of HAP formation is shifted to lower values of the extent of the reaction (α) as is also clearly illustrated by the relaxation time analysis. This heterogeneous growth of HAP is best described by a polynuclear growth model.

The combination of growth curve and relaxation time analysis is shown to be an excellent method to locate transitions in the kinetics of complex precipitating systems which are often difficult to identify in experimental relaxation curves.

APPENDIX A: CALCULATION OF SOLUTION CONCENTRATIONS

Solution concentrations of all possible complexes are calculated by considering all the equilibria in aqueous solutions involving calcium and the various hydrolysis products of phosphoric acid. On taking the logarithm of all the association constants collected in Table AI, a set of linear equations is formed (34). Using the activity of H^+ defined by pH and two trial concentrations, $[Ca^{2+}]$ and $[HPO_4^{2-}]$, this set of linear equations is solved. The concentrations of all possible complexes and the ionic strength (again in an iterative manner) are computed and used in two mass balances. Following Holt *et al.* (35) better approximations for $[Ca^{2+}]$ and $[HPO_4^{2-}]$ are found in a number of cycles to minimize the mass balances to within 0.1%. Activity coefficients were calculated with the formula proposed by Davies (36).

TABLE A1

Intrinsic Association Constants (liters mole^{-1}) and Solubility Products (mole liter^{-1})^n at 25 and 37°C

	Association constants (liters mole^{-1})			
	25°C (35)		37°C (32)	
	H^+	Ca^{2+}	H^+	Ca^{2+}
$H_2PO_4^-$	1.41×10^2 (10)	11	1.61×10^2	31.9
HPO_4^{2-}	2.84×10^7	642	1.52×10^7	681
PO_4^{3-}	2.47×10^{12}	2.88×10^6	1.51×10^{12}	3.46×10^6
OH^-	9.90×10^{13}	20	4.13×10^{13}	21.3

	Solubility products (mole liter^{-1})$^{n a}$	
	25°C (10)	37°C (32)
HAP	6.3×10^{-59}	2.35×10^{-59}
OCP	1.25×10^{-47}	5.1×10^{-50}
DCPD	2.1×10^{-7}	1.87×10^{-7}

[a] n = number of atoms in a molecule.

$$-\log f_z = Az_i^2\left[\frac{I^{1/2}}{1+I^{1/2}} - 0.3I\right], \quad \text{[A1]}$$

where f_z is the activity coefficient of a z-valent ion and I is the ionic strength of the solution. The factor A depends slightly on temperature and equals 0.51 and 0.52 at 26 and 37°C, respectively.

APPENDIX B: THE GROWTH EQUATION

A semiempirical growth equation can be derived following Nielsen (24), assuming growth of a set of monodisperse, isotropic particles. Growth can be described by following the advancement of the reaction as a function of time. If the concentration of monomers in solution is $c(0)$ at $t = 0$ and $c(t)$ at time t, then the degree of reaction α can be defined as

$$\alpha = \frac{c(0) - c(t)}{c(0) - c(\infty)}, \quad \text{[B1]}$$

where $c(\infty)$ is the saturation concentration.

The following relation between particle size (r) and the extent of the reaction (α) can be written as

$$r(t) = r(\infty)[\alpha(t)]^{1/3}, \quad \text{[B2]}$$

where $r(\infty)$ is the particle size at the end of the reaction. A relation between α and t can be derived for the different growth models:

model A: continuous growth, diffusion-controlled

model B: mononuclear growth

model C: polynuclear growth.

For pure diffusion-controlled growth (model A) the following relation for linear growth is derived by Nielsen (24, 25),

$$\dot{r} = \frac{v \cdot D}{r}(c(t) - c(\infty)) \quad \text{[B3]}$$

with v the molecular volume and D the diffusion coefficient. By using Eqs. [B1]–[B3] we derive

$$\dot{\alpha} = K_D \alpha^{1/3}(1 - \alpha) \quad \text{[B4]}$$

where

$$K_D = \frac{3v \cdot D}{r(\infty)^2}(c(0) - c(\infty)). \quad \text{[B5]}$$

In model B, the mononuclear model, it is assumed that growth proceeds via a layer

mechanism where the formation of a surface nucleus is assumed to be the rate-limiting step in the addition of a new layer to the growing crystal. The rate of advance of the layer originated by the surface nucleus is orders of magnitude larger than the frequency with which the nucleus forms.

The size-dependent rate of growth is given by (24–26)

$$\dot{r} = \beta \cdot r^2 \cdot d \cdot J_{2D}, \qquad [B6]$$

where βr^2 represents the surface area of one layer with thickness d, J_{2D} is the flux of surface nuclei, and β is a shape factor. Nielsen approximates the expression for J_{2D} by

$$J_{2D}(t) = kc(t)^m \qquad [B7]$$

with a constant value of exponent m, which is justified if the concentration $c(t)$ does not change more than one decade during the experiment. Using Eqs. [B2], [B6], and [B7] and a degree of reaction defined by

$$c(t) = c(0) \cdot (1 - \alpha(t)) \qquad [B8]$$

we derive

$$\dot{\alpha} = K_m \cdot \alpha^{4/3}(1 - \alpha)^m, \qquad [B9]$$

where

$$K_m = 3k\beta d \cdot r(\infty) \cdot c(0)^m. \qquad [B10]$$

When the relative rates of formation of a surface nucleus and its spreading across the surface are on the same order of magnitude, a polynuclear model (model c) is valid. For growth by polynuclear layers (24–26)

$$\dot{r} = 0.6(J_{2D})^{1/3} \cdot w^{2/3} \cdot d, \qquad [B11]$$

where w is the spreading velocity across the surface which is probably limited by surface diffusion

$$w = d^2 D(c(t) - c(\infty)). \qquad [B12]$$

Using Eqs. [B2], [B7], [B8], and [B11] we find

$$\dot{\alpha} = K_p \alpha^{2/3}(1 - \alpha)^p; \quad p = (m + 2)/3, \qquad [B13]$$

where

$$K_p = 1.8r(\infty)^{-1}(kd^7 D^2 c(0)^{m+2})^{1/3}. \qquad [B14]$$

For the diffusion-controlled as well as the two surface nucleation-controlled growth models the growth rate can be described by a general growth equation of the form

$$\dot{\alpha} = K\alpha^n(1 - \alpha)^m, \qquad [B15]$$

where the term α^n represents the dependence of growth rate on the surface area or size of the monodisperse particles and the term $(1 - \alpha)^m$ represents the dependence on the decreasing supersaturation during the precipitation. The rate law was derived for a set of monodisperse particles. If the precipitate is relatively polydisperse, the applicability of the rate law is limited. The development of the size distribution will depend on the value of n. If we express the growth rate in terms of the linear dimension of the isotropic particles, then

$$\dot{r} = k' r^{(3n-2)}(c(t) - c(\infty))^{m'}. \qquad [B16]$$

This expression shows that for $n = \frac{2}{3}$, the growth rate will not depend on the particle size and the size distribution will not change in time during polynuclear growth. For mononuclear growth ($n = \frac{4}{3}$) the polydispersity will increase in time whereas during diffusion-controlled growth ($n = \frac{1}{3}$) the particles will become more monodisperse while growth proceeds.

ACKNOWLEDGMENTS

This investigation was supported financially by the NIZO, Ede, The Netherlands. We also thank J. Pieters for his assistance in the electron microscopic analysis.

REFERENCES

1. Pyne, G. T., and Mc Gann, T. C. A., *J. Dairy Res.* **27,** 9 (1960).
2. Schmidt, D. G., *in* "Developments in Dairy Chemistry" (P. F. Fox, Ed.), Vol. 1, p. 61. Applied Science Pub., Barking, Essex, 1982.
3. Holt, C., *J. Dairy Res.* **49,** 29 (1982).
4. Holt, C., Hasnain, S. S., and Hukins, D. W. L., *Biochim. Biophys. Acta* **719,** 299 (1982).
5. Chaplin, L. C., *J. Dairy Res.* **51,** 251 (1984).
6. Posner, A. S., and Betts, F., *Acc. Chem. Res.* **8,** 273 (1975).
7. Termine, J. D., and Eanes, E. D., *Calcif. Tissue Res.* **10,** 171 (1972).
8. Blumenthal, N. C., and Posner, A. S., *Calcif. Tissue Res.* **13,** 235 (1973).

9. Abbona, F., Madsen, H. E. L., and Boistelle, R., *J. Cryst. Growth* **74,** 581 (1986).
10. Feenstra, T. P., and de Bruyn, P. L., *J. Phys. Chem.* **83,** 475 (1979).
11. Feenstra, T. P., Doctoral thesis, Utrecht, 1980.
12. Van Straten, H. A., Doctoral thesis, Utrecht, 1984.
13. Madsen, H. E. L., and Thorvardarson, G., *J. Cryst. Growth* **66,** 369 (1984).
14. Meyer, J. L., and Eanes, E. D., *Calcif. Tissue Res.* **25,** 209 (1978).
15. Füredi-Milhofer, H., Brečević, L., and Purgarić, B., *Faraday Discuss. Chem. Soc.* **61,** 184 (1976).
16. Koutsoukos, P. G., and Nancollas, G. H., *J. Cryst. Growth* **53,** 10 (1981).
17. De Rooij, J. F., Heughebaert, J. C., and Nancollas, G. H., *J. Colloid Interface Sci.* **100,** 350 (1984).
18. Vermeulen, A. C., Geus, J. W., Stol, R. J., and de Bruyn, P. L., *J. Colloid Interface Sci.* **51,** 449 (1975).
19. Ostwald, W., *Z. Phys. Chem.* **22,** 289 (1897).
20. Nelson, D. G. A., Salimi, H., and Nancollas, G. H., *J. Colloid Interface Sci.* **110,** 32 (1986).
21. Stranski, I. N., and Totomanov, D., *Z. Phys. Chem.* A **163,** 399 (1933).
22. Gutzow, I., and Toschev, S., *Krist. Tech.* **3,** 485 (1968).
23. Toschev, S., *in* "Crystal Growth, an Introduction" (P. Hartman, Ed.). North-Holland, Amsterdam, 1973.
24. Nielsen, A. E., *in* "Kinetics of Precipitation." Pergamon, New York, 1964.
25. Nielsen, A. E., *J. Cryst. Growth* **67,** 289 (1984).
26. Chernov, A. A., *in* "Modern Crystallography III, Crystal Growth" (A. A. Chernov, Ed.). Springer-Verlag, Berlin, 1984.
27. Nielsen, A. E., and Söhnel, O., *J. Cryst. Growth* **11,** 233 (1971).
28. Söhnel, O., *J. Cryst. Growth* **57,** 101 (1982).
29. Gilmer, G. H., and Bennema, P., *J. Appl. Phys.* **43,** 1347 (1972).
30. Boskey, A. L., and Posner, A. S., *J. Phys. Chem.* **80,** 40 (1976).
31. Pei-Tak Cheng, and Pritzker, K. P. H., *Calcif. Tissue Int.* **35,** 596 (1983).
32. Heughebaert, J. C., and Nancollas, G. H., *J. Phys. Chem.* **88,** 2478 (1984).
33. Termine, J. D., Peckauskas, R. A., and Posner, A. S., *Arch. Biochem. Biophys.* **140,** 318 (1970).
34. Feenstra, T. P., *J. Chem. Ed.* **56,** 104 (1979).
35. Holt, C., Dalgleish, D. G., and Jenness, R., *Anal. Biochem.* **113,** 154 (1981).
36. Davies, C. W., "Ion Association." Butterworth, London, 1962.